Synergistic Integration of Layer-by-Layer Assembly of Photosensitizer and Gold Nanorings for Enhanced Photodynamic Therapy in the Near Infrared

Yue Hu,[†,§] Yamin Yang,[‡,§] Hongjun Wang,[*,‡] and Henry Du[*,†]

[†]Department of Chemical Engineering and Materials Science and [‡]Department of Chemistry, Chemical Biology, and Biomedical Engineering, Stevens Institute of Technology, Hoboken, New Jersey 07030, United States. [§]These authors contributed equally.

ABSTRACT A layer-by-layer (LbL) assembly strategy was used to incorporate high concentrations of Al(III) phthalocyanine chloride tetrasulfonic acid ($AlPcS_4$) photosensitizer (PS) onto plasmonic Au nanorings (Au NRs) for increasing the cellular uptake of $AlPcS_4$ and subsequently enhancing the efficacy of photodynamic therapy (PDT) of human breast cancer cells (MDA-MB-231) in the near-infrared (NIR) range. Au NRs with two layers of $AlPcS_4$ (Au NR/$(AlPcS_4)_2$) markedly increased the cellular internalization of $AlPcS_4$ and elevated the generation of reactive oxygen species (ROS). Quenching the photosensitivity of $AlPcS_4$ on the Au NR surface during the uptake and then significant ROS formation only upon PS release inside the cellular compartment made it possible to achieve a high PDT specificity and efficacy. PDT of breast cancer cells following 4 h of incubation with various formula revealed the following cell destruction rate: ~10% with free $AlPcS_4$, ~23% with singly layered Au NR/$(AlPcS_4)_1$ complex, and ~50% with doubly layered Au NR/$(AlPcS_4)_2$. Incubation with Au NR/$(AlPcS_4)_2$ for an additional 2 h resulted in ~85% cell killing, more than 8-fold increase compared to $AlPcS_4$ alone. Together, integration of LbL of PS with Au NRs holds a significant promise for PDT therapeutic treatment of a variety of cancers.

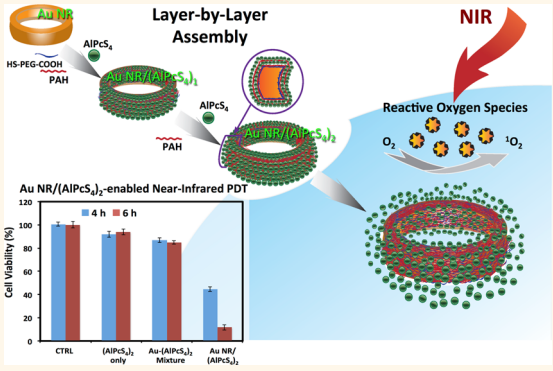

KEYWORDS: gold nanorings · plasmonic · layer-by-layer assembly · photodynamic therapy · near infrared

Photodynamic therapy (PDT), as a non-invasive therapeutic modality involving the use of photosensitizer (PS) and light irradiation, is being increasingly explored for its utility in treating malignant diseases such as cancer.[1−4] During the PDT, PS is elevated to its excited state by light irradiation, and then subsequent energy transfer to molecular oxygen results in the formation of reactive oxygen species (ROS) composed mainly of singlet oxygen ($^1O_2$).[5−7] The highly oxidizing ROS can induce apoptosis and necrosis of neoplasia cells and ultimately lead to cell destruction. While PDT is a FDA-approved therapeutic method, its broader clinical acceptance for cancer therapy would critically depend on the progresses in such areas as target delivery of high doses of PS to diseased tissues and adoption of long-wavelength light irradiation (*e.g.*, near-infrared (NIR) light) for increasing treatment depth[8] so as to overcome the challenges associated with PS instability,[9] low PS uptake by target cells,[10,11] and limited PS activation deep in the diseased tissue due to high attenuation of light in the visible range.[12]

With respect to further improvement of PDT efficacy, there is a growing interest in using Au nanostructures as a carrier for PS delivery, taking advantage of the versatile surface functionality of Au for PS conjugation, relative easy cellular uptake of Au nanoparticles, and their recognized biocompatibility.[13−15] Furthermore, the strong electromagnetic (EM) field induced by localized surface plasmon resonance (LSPR) of Au nanostructures can be harvested to enhance ROS generation, affording additional benefit for PDT treatment.[16−18] For

* Address correspondence to hdu@stevens.edu, hongjun.wang@stevens.edu.

Received for review February 2, 2015 and accepted August 12, 2015.

Published online August 12, 2015
10.1021/acsnano.5b03063

instance, chemical conjugation of PS onto colloidal Au nanoparticles allows the delivery of PS to deep cancerous tissues and therefore increases the PDT treatment depth.[19] The chemical conjugation approach is, however, limited to low PS concentration due to instability of Au colloidal solution at higher PS concentrations. In addition, PDT under NIR irradiation with the aid of Au nanorods that exhibit overlapping LSPR has proven to yield high treatment efficacy over a greater tissue depth.[20,21] This significant finding stems from a larger tissue penetration depth with NIR compared to the visible light. Note that there are two LSPR modes in an Au nanorod, a transverse mode at the two ends with a strong EM field in the NIR and a longitudinal mode along the length of the rod with a weak field in the visible. This uneven field distribution does not allow effective use of all available Au surface and PS conjugates for field-enhanced PDT. In this regard, a strategy that enables the increased PS loading in Au nanostructures while synergistically exploiting the LSPR in the NIR to the fullest extent, thus circumventing the limits of chemical conjugation of PS and the anisotropic Au nanorods, will significantly advance Au nanostructure-enhanced PDT for cancer therapy.

Here, we report the use of an intriguing Au nanostructure, Au nanoring (Au NR), as both a carrier for PS incorporated onto the Au NR surface via layer-by-layer (LbL) assembly and an EM field enhancer to enhance ROS formation at NIR, for improved PDT of breast cancer cells. The use of Au NRs offers numerous advantages. First, our earlier experimental studies have demonstrated the LSPR of Au NRs could be readily tuned to the NIR range by adjusting their size and aspect ratio.[22] Second, Au NRs allow the inner and the outer surfaces to be accessible for LBL PS loading, compared to only the outer surface of the enclosed Au nanoshells that are also known for their tunable LSPR in the NIR. Third, Au NRs are anticipated to exhibit higher EM field enhancement than nanoshells of the same dimension due to their lower mass and hence reduced radiation damping.[23] Forth, the high chemical purity of Au NRs is of great appeal for their application in PDT, compared to Au nanoshells with cytotoxic residual Ag content due to incomplete galvanic exchange with Ag nanoparticles for structural stability[24] or silica core/Au shell nanostructures where silica remains as part of the structure.[25]

LbL, sequential and alternating deposition of constituent polyelectrolytes and charged molecules, offers a powerful means of incorporating a significant amount of drugs while preserving their bioactivity.[26,27] Examples include its use to incorporate therapeutic drugs on polymeric nanoparticles for systemic delivery at high doses.[28−30] In this study, we innovatively explored the LbL method to incorporate high concentrations of Al(III) phthalocyanine chloride tetrasulfonic acid ($AlPcS_4$), a second-generation PS with a high ROS yield,[31,32] onto Au NRs for improved PDT efficacy. Our general strategy is depicted in Scheme 1. Two layers of negatively charged $AlPcS_4$ were alternatively deposited onto Au NRs by LbL via electrostatic attraction with positively charged poly(allylamine hydrochloride) (PAH) polyelectrolyte as the counterions, leading to the formation of Au NR−$AlPcS_4$ complexes. We show that a significant amount of $AlPcS_4$ could be loaded into the assembled complex, which in turn led to a marked increase of the intracellular $AlPcS_4$ level after cellular uptake of the complexes. We revealed that the photosensitivity of $AlPcS_4$ at the Au NR surface was inhibited due to charge-transfer-induced quenching.[33] Subsequent release of $AlPcS_4$ from Au NR surface after cellular internalization made the PS highly photoactive. We demonstrated that upon NIR light irradiation, the Au NR−$AlPcS_4$ complexes in the cellular compartments yielded elevated ROS formation, resulting in an 8-fold increase in cancer cell killing efficiency during PDT, compared to the use of $AlPcS_4$ only or the Au NR-$AlPcS_4$ mixture.

Scheme 1. Synergistic Integration of LbL Assembly with Au NRs for Increased Loading of PS (*i.e.*, $AlPcS_4$) and Enhanced PDT of Cancer Cells in the NIR[a]

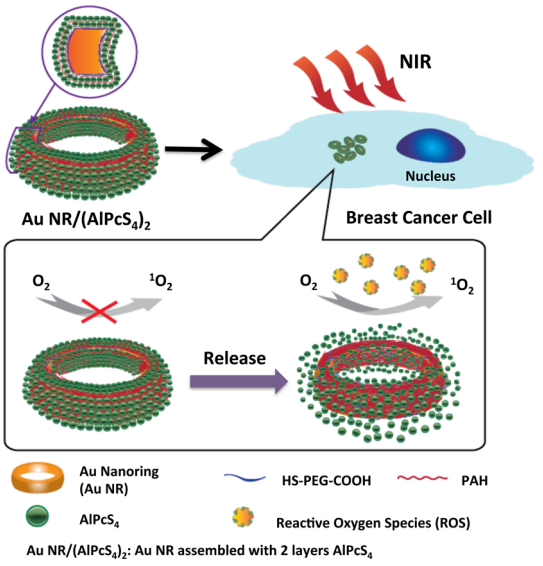

[a] The photosensitivity of $AlPcS_4$ and hence ROS formation is inhibited when the PS is directly adsorbed on the Au NR surface due to quenching effect. Field-enhanced ROS generation is activated upon release of the PS from and in the immediate vicinity of the Au NRs during NIR irradiation.

RESULTS AND DISCUSSION

Colloidal Au NRs were prepared by galvanic replacement reaction.[22] Cobalt nanoparticles (Co NPs) stabilized with poly(vinylpyrrolidone) (PVP) and sodium citrate were used as the sacrificial template, which was galvanically replaced with gold acid to form highly monodisperse and pure Au NRs. By controlling the size of Co NPs and the concentration of gold acid, both outer and inner diameters of Au NRs can be

readily modulated. In this study, an outer diameter of 30−40 nm was chosen for the synthesized Au NRs in order to achieve an optimal cellular uptake.[34] As shown in Figure 1, the as-prepared Au NRs had an average outer diameter (*D*) of 32.9 ± 2.4 nm, inner diameter (*d*) of 15.7 ± 2.5 nm, and sidewall height (*h*) of 13.4 ± 1.4 nm, respectively. Tethering neutrally charged PVP and negatively charged citrate, predominantly PVP, onto Au NRs during the synthesis yielded Au NRs with a slightly negative ζ potential of −3.4 mV. In order to facilitate the adsorption of negatively charged $AlPcS_4$ onto Au NRs illustrated in Figure 2a, thiol-terminated poly(ethylene glycol) ligand with carboxyl group (HS-PEG-COOH) at the terminal end was first introduced to the Au NR surface via ligand exchange.[35] During the exchange process, the PEG ligand could replace PVP and citrate ions originally capped on Au NRs via thiol chemistry, forming a relatively strong Au−S bond.[36] The negatively charged carboxyl group of ligands could effectively prevent the aggregation of Au NRs during the exchange. Note that a broadening of the absorption peak was observed for Au NR after PEGylation (Figure 2b) and can be attributed to slight aggregation of the Au NRs upon PEGylation that involved purification via centrifugation at 15,000 rpm and redispersion in Milli-Q water. Afterward, a layer of cationic poly(allylamine hydrochloride) (PAH) was adsorbed to switch the surface charge of Au NRs to positive for subsequent deposition of a layer of $AlPcS_4$ molecule via electrostatic interaction.

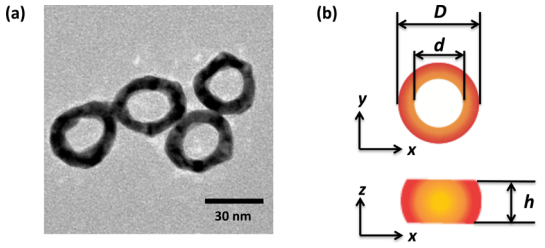

Figure 1. (a) TEM images of as-fabricated Au NRs and (b) schematic illustration of the geometry of Au NR, where *D* is the outer diameter, *d* is the inner diameter, and *h* is the sidewall height.

Adsorption of each layer onto Au NRs could be easily ascertained by the change of surface charge reflected in the measured ζ potential values. As shown in Figure 2c, following the order of as-prepared Au NRs, Au NR + PEG, Au NR + PEG + PAH and Au NR + PEG + PAH + $AlPcS_4$ (*i.e.*, Au NR/$(AlPcS_4)_1$), the measured potentials are −3.4, −34.5, + 41.3, and −29.4 mV, respectively, corresponding well with the adsorption of each layer. The switch of ζ potential from positive (Au NR + PEG + PAH) to negative (Au NR/$(AlPcS_4)_1$) indicates the robustness of electrostatic interaction in forming the Au NR−$AlPcS_4$ complexes. In addition, successful adsorption of $AlPcS_4$ onto positively charged Au NR + PEG + PAH surface was also confirmed with the appearance of the characteristic absorbance peak at 675 nm from the absorption spectrum measurement (Au NR/$(AlPcS_4)_1$ in Figure 2b). Since the $AlPcS_4$ layer completely switches the ζ potential of Au NR complexes to negative, it is possible to continue the LbL assembly, *i.e.*, alternating the deposition of PAH and $AlPcS_4$ layers, to incorporate more $AlPcS_4$. During the

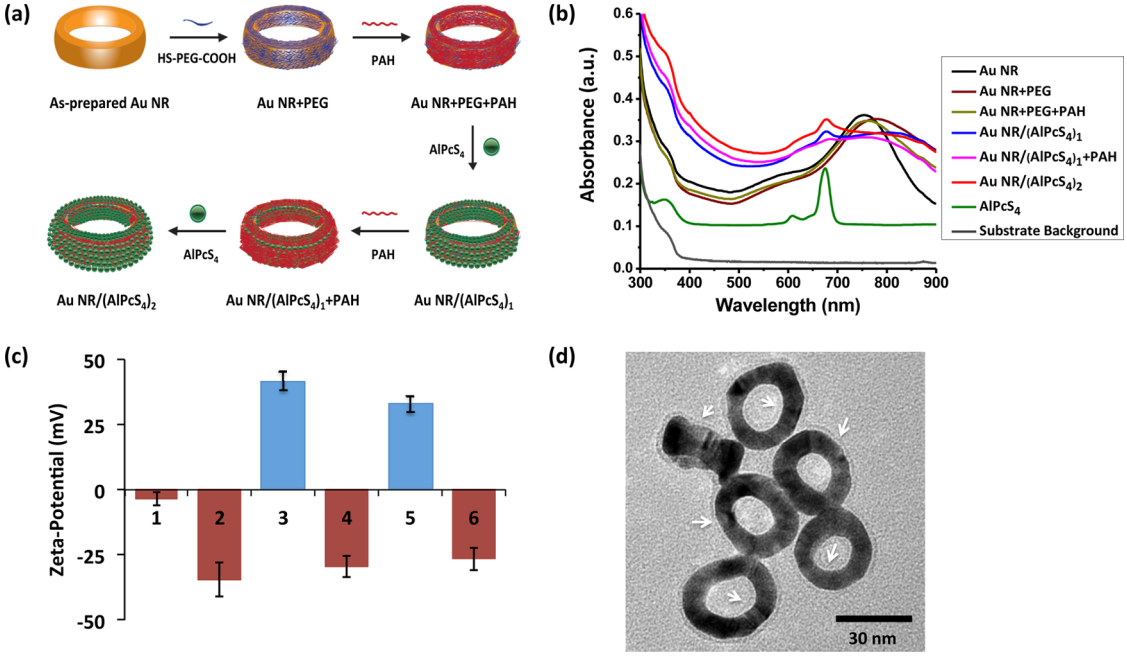

Figure 2. (a) Schematic illustration of LbL assembled $AlPcS_4$ on Au NR, leading to Au NR/$(AlPcS_4)_2$ complexes; (b) UV−vis absorption spectra of various Au NR complexes; (c) ζ potential measurements of (1) as-fabricated Au NR, (2) Au NR + PEG, (3) Au NR + PEG + PAH, (4) Au NR/$(AlPcS_4)_1$, (5) Au NR/$(AlPcS_4)_1$ + PAH, and (6) Au NR/$(AlPcS_4)_2$; and (d) TEM micrographs of Au NR/$(AlPcS_4)_2$ complexes with the LbL assembled PAH/$AlPcS_4$ layers throughout the Au NR surface as indicated by arrows.

deposition of the second PAH layer, the competitive interaction between free PAH (PAH solution) and first PAH layer of Au NR complex for $AlPcS_4$ led to partial desorption of earlier adsorbed $AlPcS_4$, as evidenced by the reduced intensity of $AlPcS_4$ peak in the absorption spectrum after the LbL deposition of the second PAH layer (Au NR/$(AlPcS_4)_1$ + PAH in Figure 2b). Partial salvaging of prior adsorbed layer is a common phenomenon during the LbL deposition of polyelectrolytes in consideration of the systematic ionic equilibrium driven by the overall entropy change.[37] Once again, the net ζ potential of the resultant Au NR/$(AlPcS_4)_1$ + PAH complex was +32.5 mV, indicating the successful deposition of the positively charged PAH on the first $AlPcS_4$ layer. Following a similar manner to the first $AlPcS_4$ deposition, a second layer of $AlPcS_4$ was also deposited onto the second PAH layer. The final resultant complex was Au NR/$(AlPcS_4)_1$ + PAH + $AlPcS_4$ (*i.e.*, Au NR/$(AlPcS_4)_2$). In the absorption spectra, the higher intensity in Au NR/$(AlPcS_4)_2$ (red in Figure 2b) is a clear indication of more $AlPcS_4$ being loaded, as compared to Au NR/$(AlPcS_4)_1$ (blue in Figure 2b). Note the concentrations of Au NRs in both Au NR/$(AlPcS_4)_1$ and Au NR/$(AlPcS_4)_2$ solutions are comparable, with a similar peak intensity of Au NRs at 802 nm.

The absorption spectra of Au NR/$(AlPcS_4)_1$, Au NR/$(AlPcS_4)_1$ + PAH, and Au NR/$(AlPcS_4)_2$ in the visible range exhibit stronger signal than the others in the corresponding wavelength. It could be attributed to the fact that the absorption spectra of these complexes in the visible range are a superposition of the spectra of the constituent Au NRs and photosensitizer $AlPcS_4$. As $AlPcS_4$ in aqueous solution shows a noticeable absorption peak in the visible range from 300 to 400 nm in Figure 2b, similar to an earlier study,[38] it will contribute to the higher signal intensity in the Au NR−$AlPcS_4$ complex. The increased signal intensity of Au NR/$(AlPcS_4)_1$, Au NR/$(AlPcS_4)_1$ + PAH, and Au NR/$(AlPcS_4)_2$ is therefore expected, particular from 400 to 500 nm. In addition, $AlPcS_4$ deposition increases the index of refraction surrounding Au NRs, leading to a slight red shift in the surface plasmon resonance of Au NRs complexes (Figure 2b).[39]

Besides ζ potential and absorption measurements, the size and morphology of Au NR/$(AlPcS_4)_2$ structures were also characterized by transmission electron microscopy (TEM). As shown in Figure 2d, the overall assembled layers laden with two depositions of $AlPcS_4$ uniformly cloaked the entire surface of Au NRs with a thickness of approximately 2 nm in all dimensions, indicating the highly controllable nature of the LbL assembly process. In principle, more $AlPcS_4$ layers can be repeatedly built into the assembled structures by LbL alternating the PAH/$AlPcS_4$ deposition steps. However, due to successive loss of Au NR/$(AlPcS_4)_n$ during purification via centrifuge at each step of the LbL processes, only up to two layers of PAH/$AlPcS_4$ depositions were pursued. Consequently, only Au NR/$(AlPcS_4)_1$ and Au NR/$(AlPcS_4)_2$ complexes were used for further experiments.

To quantify the amount of $AlPcS_4$ incorporated in the assembled Au NR−$AlPcS_4$ complexes, supernatants collected from each step of the LbL assembly were measured for their absorbance intensity at 675 nm and calculated for free $AlPcS_4$ in the solutions using the established UV−vis calibration curve (Table S1 and Figure S1). The amount of $AlPcS_4$ bound to Au NRs was calculated by subtracting the free $AlPcS_4$ from the total loaded one. On average, the molar ratio of bound $AlPcS_4$ per Au NR for Au NR/$(AlPcS_4)_1$ and Au NR/$(AlPcS_4)_2$ was ~5000:1 and ~10,000:1, respectively. Doubling the molar ratio of $AlPcS_4$ upon the second layer deposition is a strong indication of the controllability and efficiency of LbL assembly for PS loading.

There is strong evidence in the open literature about the quenching characteristics of Au nanostructures via Förster resonance energy transfer (FRET) that depends on the geometric features of Au nanostructures and their distance with fluorophore.[40] Taking advantage of this unique feature, it is possible to design the Au NR−$AlPcS_4$ complexes so that they exhibit delayed ROS formation by $AlPcS_4$ prior to their uptake by targeted cells, optimizing the PDT specificity and efficiency as a result. It is known that $AlPcS_4$ has its main absorption peak at 675 nm (Figure 2b) and its emission at 690 nm. Substantial overlap of these peaks with the LSPR (max@760 nm) of Au NRs, in conjunction with a precise control of the distance of $AlPcS_4$ from Au NR surface during LbL assembly, can facilitate the energy transfer from excited $AlPcS_4$ to Au NRs for ground-state complex formation,[41] leading to inhibited fluorescence and photosensitivity. Indeed, our measurements showed that the fluorescence of $AlPcS_4$ in both Au NR/$(AlPcS_4)_1$ and Au NR/$(AlPcS_4)_2$ complexes was markedly lower than that of either free $AlPcS_4$ or the mixed Au NRs and $AlPcS_4$ at the same concentration (Figure 3a), indicating fluorescence quench within Au NR−$AlPcS_4$ complexes. As shown in Figure 3a, the fluorescence quench of the Au NR/$(AlPcS_4)_2$ complex was more pronounced than Au NR/$(AlPcS_4)_1$. In addition to the FRET effect, the second PAH overlayer introduced on the first layer of $AlPcS_4$ during LbL facilitates more nonradiative energy transfer between $AlPcS_4$ and PAH owing to dipole−dipole interaction,[42] leading to stronger fluorescence quench observed in Au NR/$(AlPcS_4)_2$ complex as compared to Au NR/$(AlPcS_4)_1$. In ROS generation, a mixture of 1.5 μM $AlPcS_4$ and 0.15 nM Au NRs with the same concentrations as Au NR/$(AlPcS_4)_2$ was compared with Au NR/$(AlPcS_4)_2$. ROS formation was indirectly quantified by a global ROS tracking probe of dihydrorhodamine 123 (DHR123).[43] Note that cell-free ROS formation in Au NR-$(AlPcS_4)_2$ mixture and Au NR/$(AlPcS_4)_2$ complex was detected immediately after mixing with DHR123,

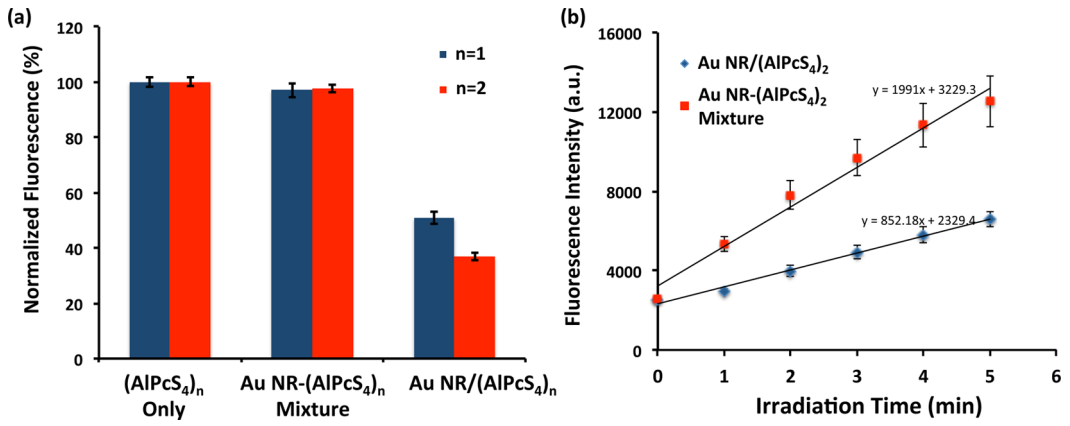

Figure 3. (a) Normalized fluorescence intensity (ex/em: 660/690 nm) of $(AlPcS_4)_n$ only, $(AlPcS_4)_n$ mixed with Au NR and Au NR/$(AlPcS_4)_n$ [where n = 1 (0.75 μM $AlPcS_4$) or 2 (1.5 μM $AlPcS_4$) and 0.15 nM Au NR equiv]; and (b) kinetic ROS formation of $AlPcS_4$ upon mixing with Au NR and Au NR/$(AlPcS_4)_2$ with detection agent DHR123. The data were collected from experiments that were repeated at least 3 times.

before dissociation of $AlPcS_4$ from Au NR surface. Although both circumstances exhibited an irradiation-dependent ROS formation, Au NR/$(AlPcS_4)_2$ demonstrated a significantly lower ROS generation rate (Figure 3b), suggesting delayed ROS formation with $AlPcS_4$ tethered onto Au NRs. The ability for $AlPcS_4$ in the Au NR/$(AlPcS_4)_2$ not to participate in ROS generation unless released from the Au NR surface due to quenching is essential to prolong the $AlPcS_4$ stability without self-destruction.

The colloidal dispersibility of Au NR/$(AlPcS_4)_1$ and Au NR/$(AlPcS_4)_2$ complexes in culture medium was also examined by dynamic light scattering (DLS) and UV–vis measurements (Table S2 and Figure S2). The Au NR–$AlPcS_4$ complexes were well-dispersed in the culture medium with negligible aggregation, as indicated by small size deviation and narrow absorption band. The biocompatibility of Au NR/$(AlPcS_4)_1$ and Au NR/$(AlPcS_4)_2$ to human breast cancer cells (MDA-MB-231) was evaluated by culturing at different concentrations for 24 h. The thiazolyl blue tetrazolium bromide (MTT) assays revealed negligible cytotoxicity of both complexes to MDA-MB-231 at 0.15 nM for 24 h (Figure S3). Interestingly, dark toxicity was only observed for Au NR/$(AlPcS_4)_2$ when the Au NRs loading concentration reached 0.25 nM due probably to a combination of high Au NRs concentration and high $AlPcS_4$ dose. Intracellular distribution of Au NR/$(AlPcS_4)_1$ or Au NR/$(AlPcS_4)_2$ upon uptake by MDA-MB-231 cells was visualized by TEM examination of the ultrathin sections of the cells incubated with these complexes for 4 h. A majority of the Au NR–$AlPcS_4$ complexes were found in the cytosolic vesicles, *i.e.*, endosomes and lysosomes, as aggregates (Figure 4 and Figure S4), indicating that internalization of Au NR/$(AlPcS_4)_1$ and Au NR/$(AlPcS_4)_2$ follows the endocytosis pathway.[44]

Upon cellular uptake, the intracellular distribution of $AlPcS_4$ could be directly visualized under the fluorescence microscope. Representative fluorescence images

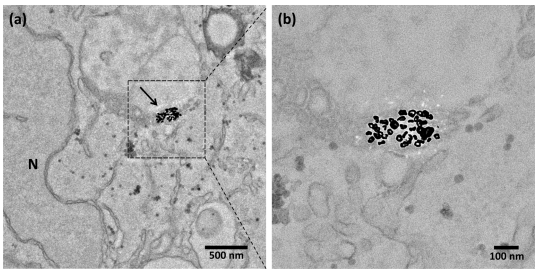

Figure 4. TEM micrographs of intracellular location of Au NR/$(AlPcS_4)_2$ (arrow) in MDA-MB-231. N stands for nucleus.

of MDA-MB-231 cells incubated with $AlPcS_4$ or Au NR–$AlPcS_4$ complexes as described in Figure 5a–f were taken at 4 and 6 h. Compared to $AlPcS_4$, the Au NR–$AlPcS_4$ complexes showed a stronger fluorescence intensity inside the cells, indicating the efficiency of Au NRs as carrier for enhancing the cellular uptake of $AlPcS_4$, in good agreement with previous findings.[45] Clearly, with the same amount of Au NRs, the fluorescence from Au NR/$(AlPcS_4)_2$ was much brighter than Au NR/$(AlPcS_4)_1$, correlating well with the initial $AlPcS_4$ loaded within the LbL assembled layer. The fluorescence intensity was also measured quantitatively which will be further discussed. It is necessary to mention that the measured fluorescence may come mainly from the $AlPcS_4$ outside of the quenching zone (a few nanometers) of the Au NR–$AlPcS_4$ complexes. To affirm this, we further extended the incubation time of the above culture for two more hours in fresh medium. Indeed, much stronger fluorescence was observed from Au NR/$(AlPcS_4)_2$ upon further 2 h incubation than the initial 4 h even after removal of the released $AlPcS_4$. While the extended culture of Au NR/$(AlPcS_4)_1$ yielded only marginal difference from the initial culture, due probably to the different release profiles between Au NR/$(AlPcS_4)_1$ and Au NR/$(AlPcS_4)_2$. To better understand the intracellular localization of Au NR–$AlPcS_4$ complexes, Lysotracker Red DND-99 was used to track the

position of endo/lysosome.[46] As shown in Figure 5b,c,e,f, fluorescence images of Au NR−$AlPcS_4$ complex-loaded cells overlapped well with Lysotracker Red DND-99 stained areas. These results indicate the colocalization between Au NR/$AlPcS_4$ complex and endo/lysosome. In contrast, in the cells treated with $AlPcS_4$ only (Figure 5a,d), $AlPcS_4$ was freely distributed in the cytoplasm, and only partially overlapped with Red DND-99-stained area. This finding further confirms that the intracellular location of the majority of the Au NR−$AlPcS_4$ complexes were in the endo/lysosomes.

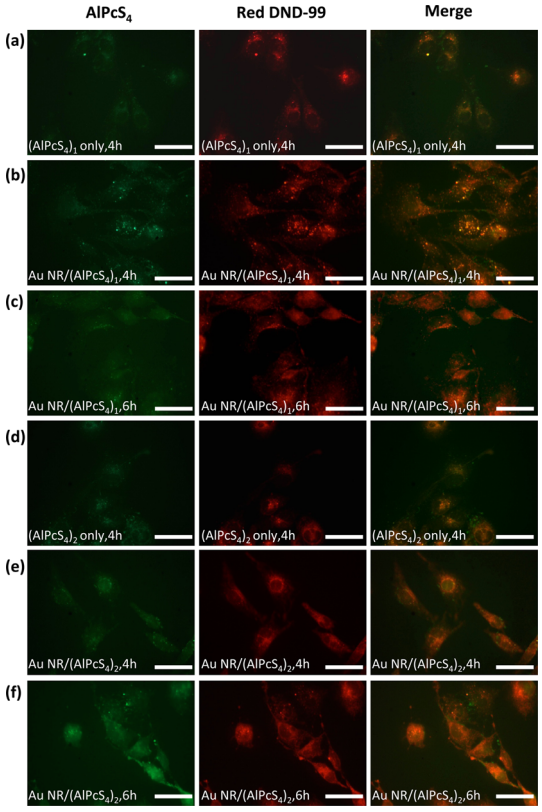

Figure 5. Representative fluorescence images of MDA-MB-231 cells incubated with $AlPcS_4$ only [(a) 0.75 μM; (d) 1.5 μM] and Au NR−$AlPcS_4$ complexes [(b) Au NR/$(AlPcS_4)_1$ at 0.75 μM $AlPcS_4$; (e) Au NR/$(AlPcS_4)_2$ at 1.5 μM $AlPcS_4$]. After incubation for 4 h, the cells were washed with HBSS and then cultured with fresh culture medium for another 2 h (c, f). After the times indicated, cells were stained with Lysotracker Red DND-99. The fluorescence images were captured at both 4 and 6 h. Left column: $AlPcS_4$, middle column: Red DND-99, and right column: merged images of $AlPcS_4$ and Red DND-99. Scale bar = 50 μm.

To quantify the differential cellular uptake of $AlPcS_4$ only or Au NR/$(AlPcS_4)_2$, fluorescence intensity of intracellular $AlPcS_4$ was also measured at different times (Figure 6a,b). As expected, the fluorescence intensity of Au NR/$(AlPcS_4)_2$ was higher than the one of Au NR/$(AlPcS_4)_1$ after 4 h incubation and further increased with the extension of incubation time, while a comparable or slightly declined fluorescence intensity was detected with $(AlPcS_4)_1$ only, $(AlPcS_4)_2$ only, and Au NR/$(AlPcS_4)_1$ groups. After 6 h incubation, the fluorescence intensity of Au NR/$(AlPcS_4)_2$ was about 2.5 times of that from $AlPcS_4$ only, further confirming the fluorescence microscopic results. The Au NR/$(AlPcS_4)_2$ complexes thus offer a more efficient approach to deliver $AlPcS_4$ to MDA-MB-231 breast cancer cells via endocytosis than gradient-driven passive diffusion.[47] In addition, $AlPcS_4$ was released from the internalized Au NR/$(AlPcS_4)_2$ in a time-dependent manner (4 vs 6 h).

The ability of LbL assembled coating for controlled release of small molecule was demonstrated[48−50] but was not tested for Au NR−$AlPcS_4$ complexes. In this regard, further analysis of the $AlPcS_4$ release from individual complexes is necessary. As shown in Figure 6c, about 80% of the bound $AlPcS_4$ was released from Au NR/$(AlPcS_4)_2$ over a 6 h period in a physiological buffer solution (PBS), whereas a similar release percentage for Au NR/$(AlPcS_4)_1$ was reached after only 4 h of incubation under the same conditions. Similar release profile was also obtained with Au NR−$AlPcS_4$ complexes in the culture medium (Figure S5). The slower release rate of Au NR/$(AlPcS_4)_2$ can be attributed to the additional PAH overlayer introduced on the first layer of $AlPcS_4$ during LbL, acting as a barrier to reduce the diffusion of $AlPcS_4$. Taken together, tethering $AlPcS_4$ onto Au NRs through LbL assembly can not only protect $AlPcS_4$ from light decomposition and improve loading efficiency but also increase the cellular uptake

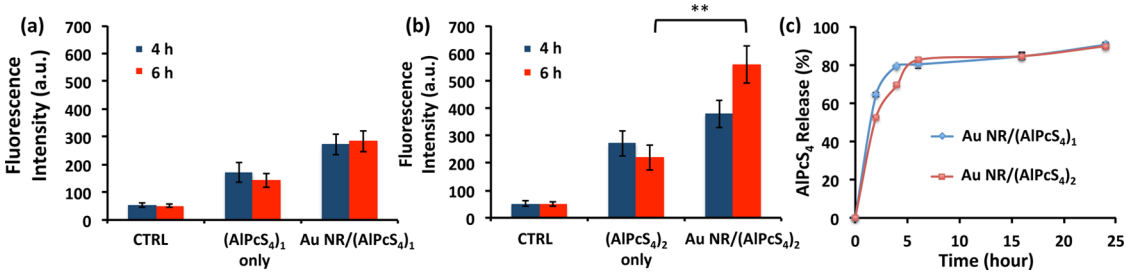

Figure 6. Intracellular $AlPcS_4$ fluorescence after incubation with $(AlPcS_4)_n$ only and Au NR/$(AlPcS_4)_n$: (a) n = 1 (0.75 μM $AlPcS_4$) and (b) n = 2 (1.5 μM $AlPcS_4$) for 4 and 6 h, respectively. A constant Au NR concentration of 1.5 nM was used for all studies. The presented data are average of three separate experiments. **$p < 0.005$. (c) The concentration of $AlPcS_4$ released from Au NR/$(AlPcS_4)_1$ and Au NR/$(AlPcS_4)_2$ as a function of time. The release was performed by suspending the complexes in PBS (pH ~ 7.4) and incubating at 37 °C under gentle shaking. The concentration of $AlPcS_4$ was calculated from fluorescence intensity measurement, and the initial loading concentration was 0.75 and 1.5 μM, respectively.

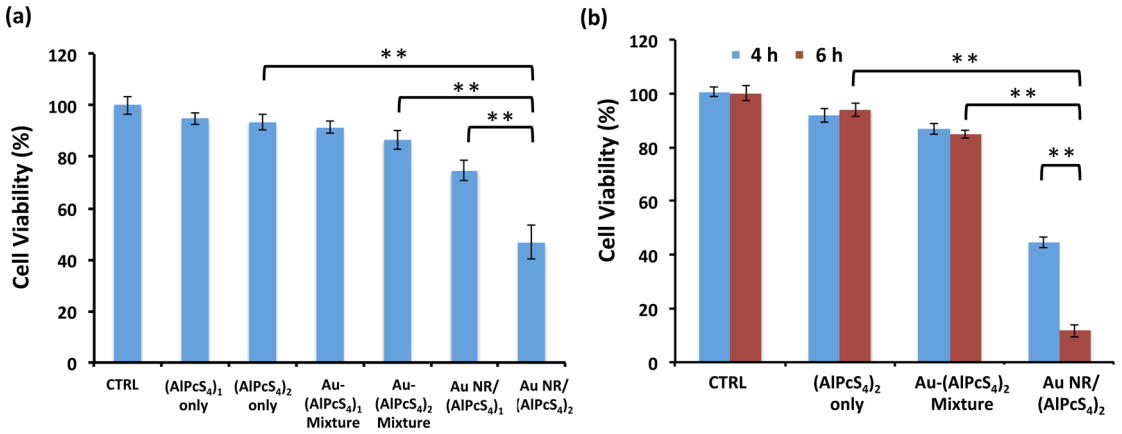

Figure 7. Quantification of MDA-MB-231 cell viability by MTT assay after various PDT treatments where cells were incubated for 4 h (a) with $AlPcS_4$ only [$(AlPcS_4)_1$: 0.75 μM and $(AlPcS_4)_2$: 1.5 μM], with Au NR-$AlPcS_4$ mixture [0.75 μM $(AlPcS_4)_1$ and 1.5 μM $(AlPcS_4)_2$,] and with Au NR−$AlPcS_4$ complexes [Au NR/$(AlPcS_4)_1$ and Au NR/$(AlPcS_4)_2$] and incubated for 4 or 6 h (b) with 1.5 μM $(AlPcS_4)_2$ only, Au NR-1.5 μM $(AlPcS_4)_2$ mixture, and Au NR/$(AlPcS_4)_2$ prior to 20 min NIR light (λ > 600 nm) irradiation. A constant Au NR concentration of 1.5 nM was used for all studies. The irradiated cells were further cultured for 24 h prior to MTT measurement. The culture without $AlPcS_4$ and Au NRs was used as controls. **p < 0.001.

efficiency of $AlPcS_4$. More importantly, the delayed release of $AlPcS_4$ from Au NR/$(AlPcS_4)_2$ can also effectively minimize the loss of $AlPcS_4$ during circulation and cell internalization. These features are highly desirable for enhanced PDT efficacy.

To investigate the effect of Au NR−$AlPcS_4$ complexes on PDT, monolayer cultured MDA-MB-231 cells were used as a model platform for PDT experiments. Previous finding has demonstrated the capability of LSPR of Au nanostructures in elevating ROS formation during PDT.[51−53] In this regard, light irradiation with NIR light close to the LSPR of Au NRs and the absorption peak of $AlPcS_4$ would be beneficial (Figure 2b). MDA-MB-231 cells after incubation with $AlPcS_4$ only, Au NR-$AlPcS_4$ mixtures, or Au NR−$AlPcS_4$ complexes were irradiated with a halogen light filtered with 600 nm long pass filter. Light intensity was significantly reduced after the long pass filter, which resulted in negligible hyperthermia destruction (data not shown). PDT treatment for those 4 h incubations with various formats of $AlPcS_4$, only Au NR−$AlPcS_4$ complexes yielded pronounced cell killing with ~23% cell destruction for Au NR/$(AlPcS_4)_1$ and ~54% for Au NR/$(AlPcS_4)_2$ at the same Au NRs concentration (Figure 7a). To clarify two possible factors contributing to the enhancement of cell destruction: (1) increased cellular delivery of $AlPcS_4$ and (2) enhanced ROS generation due to the plasmonic properties of Au NRs under light irradiation, we further compared the killing efficiency under the same treatment conditions with the same amount of $AlPcS_4$ delivered into cells using silica (SiO_2) nanoparticles as carriers (detailed information can be found in Supporting Information). Note that the two layers of $AlPcS_4$ were deposited on SiO_2 nanoparticles via the same LbL assembly strategy as for Au NR−$AlPcS_4$ complex formation, resulting in SiO_2/$(AlPcS_4)_2$. As shown in Figure S6, Au NR/$(AlPcS_4)_2$ exhibited a significant higher cell destruction rate than SiO_2/$(AlPcS_4)_2$ upon light irradiation, suggesting the significant effect of EM field enhancement in elevated ROS generation that is absent in SiO_2-based complexes. In recognition of the unique capability of Au NR/$(AlPcS_4)_2$ for continuous release of $AlPcS_4$ between 4 and 6 h, it would be essential to determine whether such an attribute could benefit PDT. Thus, MDA-MB-231 cells incubated with Au NR/$(AlPcS_4)_2$ for additional 2 h (a total of 6 h) were similarly irradiated with NIR light and evaluated for cell destruction. Strikingly, a significant cell killing (~90%) was achieved (Figure 7b). In the cell-free ROS measurement (Figure 3b), at the very early stage of Au NR−$AlPcS_4$ complexes before the release of photosensitizer $AlPcS_4$ from the Au NR surface, the quenching effect of Au NR plays a dominating role in the ROS formation. However, upon cellular uptake and incubation for 4 h, release of $AlPcS_4$ from Au NR took place efficiently (Figure 6) and reached the maximum at 6 h. Therefore, the efficient release of $AlPcS_4$ represents a major contributor to the final cell destruction with significant ROS enhancement. The high cell destruction efficacy found in the Au NR/$(AlPcS_4)_2$ treated group may result from a combinational effect of the high $AlPcS_4$ retention in cancer cells and NIR-enabled field-enhanced ROS formation.

Under NIR light irradiation, individually SERS-active Au NRs are able to generate enhanced EM field and delivery the amplified energy to sufficiently activate $AlPcS_4$ molecules and induce the formation of ROS for cell destruction. In contrast, PDT treatment after 6 h incubation with $AlPcS_4$ only or $AlPcS_4$ mixed with Au NRs at the same $AlPcS_4$ and Au NRs concentration as Au NR/$(AlPcS_4)_2$ only yielded ~10% cell killing efficiency. Clearly, Au NRs functionalized with $AlPcS_4$ via LbL assembly have the potential to be part of PDT strategy with marked improvement of killing efficiency of

breast cancer cells. Further increase in the layers of LbL assembly of $AlPcS_4$ would be beneficial for loading more $AlPcS_4$ without inducing significant phototoxicity. On the other hand, a comprehensive study on the maximal distance to quench the fluorescence and ROS formation of $AlPcS_4$ by Au NRs would give an indication of maximum layers of $AlPcS_4$ deposited onto Au NRs for optimal PDT efficacy. Despite the promising results, we are keenly aware of the importance of *in vivo* experiments in order to translate *in vitro* findings to potentially positive outcome in preclinical practice.

CONCLUSION

In summary, LbL assembly offers an effective and robust approach to deposit $AlPcS_4$ onto Au NRs with the loading amount precisely controlled by the LbL process. The resultant Au NR/$(AlPcS_4)_n$ complexes (where n = 1 or 2) prove to be far more efficient for delivering $AlPcS_4$ to cancer cells for internalization than $AlPcS_4$ itself or the mixture of $AlPcS_4$ with Au NRs. In addition, the unique quenching capability of Au NRs, *i.e.*, inhibiting the photosensitivity and hence ROS formation of bound $AlPcS_4$, better protects $AlPcS_4$ from deactivation in the process of cell uptake and internalization. The combination of delayed release of $AlPcS_4$ from Au NR/$(AlPcS_4)_2$ and NIR light irradiation results in an 8-fold increase in PDT-induced cell killing efficiency, compared to that of $AlPcS_4$ or Au NR-$AlPcS_4$ mixture-based PDT. Upon further optimization of the LbL procedure especially in conjunction with targeting mechanism for cancer cells, the multifunctional Au NR/$(AlPcS_4)_n$ complexes with NIR-LSPR have great potential to overcome the ongoing challenges associated with current clinical practice of PDT for cancer therapy by greatly improving the efficacy and tissue penetration depth.

EXPERIMENTAL METHODS

Materials. Cobalt chloride hexahydrate ($CoCl_2 \cdot 6H_2O$ 99,99%), sodium borohydride ($NaBH_4$ 99%), gold(III) chloride solution (30 wt % of $HAuCl_4$ in diluted HCl), poly(vinylpyrrolidone) (PVP, M_w = 2500), poly(allylamine hydrochloride) (PAH, M_w = 15,000), poly(ethylene glycol) 2-mercaptoethyl ether acetic acid (HS-PEG-COOH, M_w = 3,500), dihydrorhodamine-123 (DHR123), and (3-aminopropyl)trimethoxysilane (APTMS) were purchased from Sigma-Aldrich (St Louis, MO). Sodium citrate trihydrate was procured from Fisher Scientific (Pittsburgh, PA). Al(III) phthalocyanine chloride tetrasulfonic acid ($AlPcS_4$) was obtained from Frontier Scientific Inc. (Logan, UT). Silica Microspheres (SiO_2, size ~50 nm) were purchased from Polysciences, Inc. (Warrington, PA). Milli-Q ultrapure water (<18.2 MΩ·cm) was used for synthesis experiments.

Preparation of Au NRs. Au NRs were prepared using galvanic replacement reaction as described previously.[22] Briefly, a mixture of 100 μL 0.4 M $CoCl_2 \cdot 6H_2O$ and 400 μL 0.1 M sodium citrate trihydrate was added to 100 mL Milli-Q water and deaerated for 40 min. Then, 1 mL of 0.1 M freshly prepared $NaBH_4$ and 200 μL of 1 wt % PVP were injected into the solution simultaneously under vigorous mechanical stirring with continuous argon flow to prevent oxidation, resulting in the formation of Co NPs. After stirring for 40 min, 150 μL of 0.1 M $HAuCl_4$ was added into the cobalt solution dropwise and reacted for 30 min. Thereafter, the solution was exposed to the ambient environment to remove unreacted cobalt by oxidation and dissolution of cobalt oxide, thereby obtaining highly pure colloidal Au NRs.

PEGylation of Au NRs with HS-PEG-COOH. Au NR colloidal solution was centrifuged at 8000 rpm for 10 min to remove excess PVP and sodium citrate, and then Au NRs were dispersed in deionized water. In a typical process, 0.8 mL of a 0.25 mM freshly prepared HS-PEG-COOH solution was added to 5.2 mL of 1 nM Au NR colloidal solution. The mixture was stirred overnight at 4 °C. After PEGylation, the solution was centrifuged at 15,000 rpm for 15 min and redispersed in Milli-Q water for three times to remove unreacted HS-PEG-COOH.

LbL Assembly of $AlPcS_4$ onto Au NRs. For polyelectrolyte deposition, 0.1 mL of 10 mg/mL PAH and 0.1 mL of 1 mM NaCl solutions were added to 0.8 mL 1 nM PEG-Au NRs. After adsorption for 40 min, Au NRs were washed with Milli-Q water for three times. Subsequently, 0.1 mL of 100 uM $AlPcS_4$ was added to 0.9 mL of 1 nM PEG-Au NR-PAH solution and incubated for 1 h to form a charged complex. Excessive $AlPcS_4$ was removed by centrifugation and carefully collected for further evaluation. Additional PAH and $AlPcS_4$ layers were assembled following the same manner. The final purified complex was dispersed in Milli-Q water. The whole deposition process was performed under the dark conditions.

Quantification of $AlPcS_4$ on Au NRs. Prior to analysis, a UV−vis calibration curve for $AlPcS_4$ with a series of known concentrations (0.5, 1, 5, 10, and 20 μM) was obtained, in which the absorbance intensity of $AlPcS_4$ at 675 nm is linearly proportional to the concentration. To estimate the amount of $AlPcS_4$ assembled onto Au NRs, the unconjugated $AlPcS_4$ in the supernatants upon centrifugation separation of Au NR−$AlPcS_4$ complexes was determined by measuring the absorbance at 675 nm and then calculating against the $AlPcS_4$ UV−vis calibration curve. The amount of $AlPcS_4$ tethered onto Au NRs was obtained by subtracting the unconjugated $AlPcS_4$ from the total amount. Measurement was repeated at least three times.

The release of $AlPcS_4$ from Au NR−$AlPcS_4$ complexes was determined by suspending the complexes in PBS (6.7 mM, pH 7.4) at a final Au NRs concentration of 0.15 nM and then incubating at 37 °C in the dark. At designated times, the complexes were centrifuged, and supernatants were collected and measured for the absorbance intensity at 675 nm. The release curve was obtained by plotting the released $AlPcS_4$ against the incubation time.

Characterization of LbL Assembled Au NR−$AlPcS_4$ Complexes. The size, distribution, and absorption spectra of as-fabricated Au NRs and Au NR−$AlPcS_4$ complexes were examined with a TEM (Philips CM20) and a UV−vis spectrometer (Synergy HT multidetection microplate reader, BioTek Instruments, Inc., Winooski, VT). The obtained images were analyzed for size and distribution with Image-J 1.46 software (NIH). ζ potential of the Au NRs upon each layer deposition was measured with a Zetasizer Nano Z (Malvern Instruments Ltd., Worcestershire, U.K.). The colloidal dispersibility of Au NR−$AlPcS_4$ complexes in culture medium was evaluated by DLS with Zetasizer Nano Z (Malvern Instruments Ltd., Worcestershire, U.K.) and UV−vis spectrometer.

Preparation of SiO_2−$AlPcS_4$ Complexes. For the formation of SiO_2−$AlPcS_4$ complexes, the process was similar to Au NR−$AlPcS_4$ complexes. Briefly, 10 mg/mL APTMS was added into 1 mL of 50 nm SiO_2 nanoparticles solution (0.5 mg/mL of ethanol), and the final weight ratio of SiO_2:APTMS was 10:1. After 12 h of stirring at room temperature, modified silica nanoparticles were isolated and purified by centrifugation and redispersion processes (for 10 min at 15,000 rpm, 3 times) to remove the excess APTMS. The purified SiO_2-APTMS nanoparticles were dispersed in Milli-Q water with positive charge. Subsequently, $AlPcS_4$ and PAH layers were added repeatedly as described above. The final purified complex was dispersed in

Milli-Q water. The whole deposition process was performed under the dark condition.

ROS Formation. Au NR−$AlPcS_4$ complexes and free $AlPcS_4$ mixed with Au NRs were studied for ROS formation with DHR123 as a global ROS tracking agent, which turns to fluorescent Rhodamine 123 (R123) upon oxidation by ROS.[43] Briefly, 50 μL of 10 μM DHR123 was added into 100 μL of Au NR−$AlPcS_4$ complexes or the mixture of $AlPcS_4$ and Au NRs in 96-well plates (n = 3) with a final concentration of 0.15 nM Au NRs, 1.5 μM $AlPcS_4$, and 3.33 μM DHR123 was irradiated for different time durations with a 150 W halogen lamp (100 mW/cm^2, Dolan-Jenner Fiber-Lite MI-150, Dolan-Jenner Industries, MA) filtered through 600 nm long pass filter (Thorlab FEL0600). The fluorescence intensity was measured 1 min after irradiation using the Synergy HT multimode microplate reader at 485/20 nm for excitation and 528/20 nm for emission.

Cell Seeding and Culture. Human breast cancer cells (MDA-MB-231, ATCC, Manassas, VA) were used as a model in this study. The cells were cultured in L-15 medium (Leibovitz) (Life Technologies, Grand Island, NY) supplemented with 10% (v/v) fetal bovine serum (FBS, Atlanta Biologicals, Flowery Branch, GA) and 1% (v/v) 100 mM penicillin/streptomycin (Sigma-Aldrich, St. Louis, MO) at 37 °C without CO_2.

Intracellular Distribution of Au NR−$AlPcS_4$ Complexes by TEM. MDA-MB-231 cells (1.5×10^4 cells/mL) seeded onto 6-well plates and cultured for 24 h were incubated with Au NR−$AlPcS_4$ complexes suspended in serum-free medium at a final concentration of 1.5 μM $AlPcS_4$. After incubation for 4 h, the cells washed three times with PBS were typsinized and centrifuged to obtain cell pellets. The pellets were fixed with the glutaraldehyde−formaldehyde fixative (Electron Microscopy Sciences, Hatfield, PA). After fixation for 24 h, the pellets were washed with PBS and then postfixed with osmium tetroxide for 1 h. Upon rinsing with distilled water, the pellets were dehydrated in a series of graded ethanol and embedded in Epoxy for 24 h. Thin sections (60 nm) of the embedded pellets were cut with Leica Ultracut S Ultramicrotome (Leica Microsystems Inc., IL) and then examined with TEM.

Fluorescence Analysis. To study the subcellular localization of Au NR−$AlPcS_4$ complex, MDA-MB-231 cells (1.5×10^4 cells/mL) were seeded on the cover glass for 24 h. After 4 h incubation of free $AlPcS_4$ and Au NR−$AlPcS_4$ complexes at 1.5 μM and 0.75 μM $AlPcS_4$ equivalent concentrations, respectively, cells were washed three times with Hank's buffered salt solution (HBSS) in the dark and then cultured with fresh culture medium. Meanwhile, cells were stained 30 min with Lysotracker Red DND-99 (Molecular Probes, Life Technologies, Grand Island, NY) according to the manufacturer's instruction to label lysosomes inside of cells. The final working concentration of 60 nM of the Red DND-99 in the growth medium was used. Fluorescence images of cells at 4 h or after culture for another 2 h were captured using Nikon Eclipse 80i epi fluorescence microscope to observe intracellular distribution of free $AlPcS_4$, Au NR−$AlPcS_4$ complex, and Red DND-99-stained endo/lysosomes. Overlap between Au NR−$AlPcS_4$ complex and Red DND-99-stained endo/lysosomes was observed by merging the colocalization and fluorescent topographic profiles using NIS-Elements BR 3.10 software.

To determine the cellular uptake of $AlPcS_4$, MDA-MB-231 cells cultured in 96-well plates (3×10^3 cells/well) for 24 h were treated with 200 μL of free $AlPcS_4$ or Au NR−$AlPcS_4$ complexes (1.5 μM $AlPcS_4$ equivalent) in serum-free medium for 4 h at 37 °C. Thereafter, the cells were washed with HBSS for three times and added 200 μL phenol red-free L-15 medium. Fluorescence intensity of $AlPcS_4$ was measured with the Synergy HT multimode fluorescence microplate reader (ex = 660 nm, em = 690 nm).

Cellular Photodynamic Therapy (PDT). The cellular PDT was conducted following a similar procedure as reported previously.[54] Briefly, 200 μL of MDA-MB-231 cell suspension (1.5×10^4 cells/mL) for each well was seeded into 96-well plates. After 24 h, the medium of cell-seeded well plates was replaced with serum-free medium containing $AlPcS_4$ or Au NR−$AlPcS_4$ complexes or SiO_2−$AlPcS_4$ complexes at an equivalent concentration of 0.75 or 1.5 μM $AlPcS_4$. Serum-free medium was used as control. After incubation for 4 h in the dark, the medium was replaced with 100 μL of phenol red-free L-15 medium and then the cells were irradiated with a broadband light source of a 150 W halogen lamp filtered through 600 nm long-pass filter for 20 min. After irradiation, phenol red-free L-15 medium was replaced with complete cell culture media and incubated for 24 h before cell viability assessment.

Cell Viability. The viability of cells was determined by the thiazolyl blue tetrazolium bromide (MTT, Sigma) assay. Briefly, the cells after different treatments were incubated with 0.5 mg/mL MTT in cell culture medium for 2 h at 37 °C. After removal of the nonreacted MTT, 100 μL of dimethyl sulfoxide (DMSO, Sigma) was added to dissolve the formazan crystals. Absorbance of the extract was measured at 570 nm with a Synergy HT multimode microplate reader. Cell viability was calculated as a percentage of the nontreated control. Dark toxicity of free AlPcS4 or Au NR-AlPcS4 complexes was also evaluated by incubation for 24 h at an equivalent concentration without light exposure.

Statistical Analysis. Each experiment was repeated at least three times on different days and data were expressed as the mean ± standard deviation. All quantitative measurements were collected at least in triplicate for each group. Student's t test was used for statistical analysis. A value of $p < 0.05$ was considered to be statistically significant.

Conflict of Interest: The authors declare no competing financial interest.

Acknowledgment. Y.H. acknowledges support from the teaching assistantship from Stevens Institute of Technology. Y.Y. acknowledges the financial support from the Innovation & Entrepreneurship Doctoral Fellowship from Stevens Institute of Technology.

Supporting Information Available: The Supporting Information is available free of charge on the ACS Publications website at DOI: 10.1021/acsnano.5b03063.

The experimental results of control samples (PDF)

REFERENCES AND NOTES

1. Touma, D.; Yaar, M.; Whitehead, S.; Konnikov, N.; Gilchrest, B. a A Trial of Short Incubation, Broad-Area Photodynamic Therapy for Facial Actinic Keratoses and Diffuse Photodamage. *Arch. Dermatol.* **2004**, *140*, 33–40.
2. Ackroyd, R.; Kelty, C.; Brown, N.; Reed, M. The History of Photodetection and Photodynamic Therapy. *Photochem. Photobiol.* **2001**, *74*, 656–669.
3. Castano, A. P.; Mroz, P.; Hamblin, M. R. Photodynamic Therapy and Anti-Tumour Immunity. *Nat. Rev. Cancer* **2006**, *6*, 535–545.
4. Felsher, D. W. Cancer Revoked: Oncogenes as Therapeutic Targets. *Nat. Rev. Cancer* **2003**, *3*, 375–380.
5. Dougherty, T. J.; Gomer, C. J.; Henderson, B. W.; Jori, G.; Kessel, D.; Korbelik, M.; Moan, J.; Peng, Q. Photodynamic Therapy. *JNCI J. Natl. Cancer Inst.* **1998**, *90*, 889–905.
6. Huang, P.; Lin, J.; Wang, X.; Wang, Z.; Zhang, C.; He, M.; Wang, K.; Chen, F.; Li, Z.; Shen, G.; et al. Light-Triggered Theranostics Based on Photosensitizer-Conjugated Carbon Dots for Simultaneous Enhanced-Fluorescence Imaging and Photodynamic Therapy. *Adv. Mater.* **2012**, *24*, 5104–5110.
7. Henderson, B. W.; Dougherty, T. J. How Does Photodynamic Therapy Work? *Photochem. Photobiol.* **1992**, *55*, 145–157.
8. Smith, A. M.; Mancini, M. C.; Nie, S. Bioimaging: Second Window for *In Vivo* Imaging. *Nat. Nanotechnol.* **2009**, *4*, 710–711.
9. Hongying, Y.; Fuyuan, W.; Zhiyi, Z. Photobleaching of Chlorins in Homogeneous and Heterogeneous Media. *Dyes Pigm.* **1999**, *43*, 109–117.
10. Bechet, D.; Couleaud, P.; Frochot, C.; Viriot, M.-L.; Guillemin, F.; Barberi-Heyob, M. Nanoparticles as Vehicles for Delivery of Photodynamic Therapy Agents. *Trends Biotechnol.* **2008**, *26*, 612–621.
11. Sun, Y.; Chen, Z.-L.; Yang, X.-X.; Huang, P.; Zhou, X.-P.; Du, X.-X. Magnetic Chitosan Nanoparticles as a Drug Delivery

System for Targeting Photodynamic Therapy. *Nanotechnology* **2009**, *20*, 135102.
12. Yang, Y.; Yang, X.; Zou, J.; Jia, C.; Hu, Y.; Du, H.; Wang, H. Evaluation of Photodynamic Therapy Efficiency Using an *In Vitro* Three-Dimensional Microfluidic Breast Cancer Tissue Model. *Lab Chip* **2015**, *15*, 735–744.
13. Rana, S.; Bajaj, A.; Mout, R.; Rotello, V. M. Monolayer Coated Gold Nanoparticles for Delivery Applications. *Adv. Drug Delivery Rev.* **2012**, *64*, 200–216.
14. Rai, P.; Mallidi, S.; Zheng, X.; Rahmanzadeh, R.; Mir, Y.; Elrington, S.; Khurshid, A.; Hasan, T. Development and Applications of Photo-Triggered Theranostic Agents. *Adv. Drug Delivery Rev.* **2010**, *62*, 1094–1124.
15. Hone, D. C.; Walker, P. I.; Evans-gowing, R.; FitzGerald, S.; Beeby, A.; Chambrier, I.; Cook, M. J.; Russell, D. A. Generation of Cytotoxic Singlet Oxygen *via* Phthalocyanine-Stabilized Gold Nanoparticles: A Potential Delivery Vehicle for Photodynamic Therapy. *Langmuir* **2002**, *18*, 2985–2987.
16. Halas, N. J.; Lal, S.; Chang, W. S.; Link, S.; Nordlander, P. Plasmons in Strongly Coupled Metallic Nanostructures. *Chem. Rev.* **2011**, *111*, 3913–3961.
17. Shukla, R.; Bansal, V.; Chaudhary, M.; Basu, A.; Bhonde, R. R.; Sastry, M. Biocompatibility of Gold Nanoparticles and Their Endocytotic Fate inside the Cellular Compartment: A Microscopic Overview. *Langmuir* **2005**, *21*, 10644–10654.
18. Selvakannan, P.; Mandal, S.; Phadtare, S.; Pasricha, R.; Sastry, M. Capping of Gold Nanoparticles by the Amino Acid Lysine Renders Them Water-Dispersible. *Langmuir* **2003**, *19*, 3545–3549.
19. Cheng, Y.; Meyers, J. D.; Broome, A.-M.; Kenney, M. E.; Basilion, J. P.; Burda, C. Deep Penetration of a PDT Drug into Tumors by Noncovalent Drug-Gold Nanoparticle Conjugates. *J. Am. Chem. Soc.* **2011**, *133*, 2583–2591.
20. Jang, B.; Choi, Y. Photosensitizer-Conjugated Gold Nanorods for Enzyme-Activatable Fluorescence Imaging and Photodynamic Therapy. *Theranostics* **2012**, *2*, 190–197.
21. Jang, B.; Park, J.; Tung, C.; Kim, I.; Choi, Y. Gold Nanorod–Photosensitizer Complex for Near-Infrared Fluorescence Imaging and Photodynamic/Photothermal Therapy *In Vivo*. *ACS Nano* **2011**, *5*, 1086–1094.
22. Hu, Y.; Chou, T.; Wang, H.; Du, H. Monodisperse Colloidal Gold Nanorings: Synthesis and Utility for Surface-Enhanced Raman Scattering. *J. Phys. Chem. C* **2014**, *118*, 16011–16018.
23. Raschke, G.; Brogl, S.; Susha, A. S.; Rogach, A. L.; Klar, T. A.; Feldmann, J.; Fieres, B.; Petkov, N.; Bein, T.; Nichtl, A.; et al. Gold Nanoshells Improve Single Nanoparticle Molecular Sensors. *Nano Lett.* **2004**, *4*, 1853–1857.
24. Sun, Y.; Xia, Y. Increased Sensitivity of Surface Plasmon Resonance of Gold Nanoshells Compared to that of Gold Solid Colloids in Response to Environmental Changes. *Anal. Chem.* **2002**, *74*, 5297–5305.
25. Lal, S.; Clare, S. E.; Halas, N. J. Nanoshell-Enabled Photothermal Cancer Therapy: Impending Clinical Impact. *Acc. Chem. Res.* **2008**, *41*, 1842–1851.
26. Kozlovskaya, V.; Ok, S.; Sousa, A.; Libera, M.; Sukhishvili, S. a. Hydrogen-Bonded Polymer Capsules Formed by Layer-by-Layer Self-Assembly. *Macromolecules* **2003**, *36*, 8590–8592.
27. Kozlovskaya, V.; Kharlampieva, E.; Mansfield, M. L.; Sukhishvili, S. A. Poly(methacrylic Acid) Hydrogel Films and Capsules: Response to pH and Ionic Strength, and Encapsulation of Macromolecules. *Chem. Mater.* **2006**, *18*, 328–336.
28. Poon, Z.; Chang, D.; Zhao, X.; Hammond, P. T. Layer-by-Layer Nanoparticles with a pH-Sheddable Layer for *In Vivo* Targeting of Tumor Hypoxia. *ACS Nano* **2011**, *5*, 4284–4292.
29. Shutava, T. G.; Balkundi, S. S.; Vangala, P.; Steffan, J. J.; Bigelow, R. L.; Cardelli, J. A.; O'Neal, D. P.; Lvov, Y. M. Layer-by-Layer-Coated Gelatin Nanoparticles as a Vehicle for Delivery of Natural Polyphenols. *ACS Nano* **2009**, *3*, 1877–1885.
30. Peyratout, C. S.; Dähne, L. Tailor-Made Polyelectrolyte Microcapsules: From Multilayers to Smart Containers. *Angew. Chem., Int. Ed.* **2004**, *43*, 3762–3783.
31. Vrouenraets, M. B.; Visser, G. W. M.; Stigter, M.; Oppelaar, H.; Snow, G. B.; Van Dongen, G. A. M. S. Targeting of Aluminum (III) Phthalocyanine Tetrasulfonate by Use of Internalizing Monoclonal Antibodies: Improved Efficacy in Photodynamic Therapy. *Cancer Res.* **2001**, *61*, 1970–1975.
32. Fernandez, J. M.; Bilgin, M. D.; Grossweiner, L. I. Singlet Oxygen Generation by Photodynamic Agents. *J. Photochem. Photobiol., B* **1997**, *37*, 131–140.
33. Singh, M. P.; Strouse, G. F. Involement of the LSPR Spectral Overlap for Energy Transfer between a Dye and Au Nanoparticle. *J. Am. Chem. Soc.* **2010**, *132*, 9383–9391.
34. Jiang, W.; Kim, B. Y. S.; Rutka, J. T.; Chan, W. C. W. Nanoparticle-Mediated Cellular Response Is Size-Dependent. *Nat. Nanotechnol.* **2008**, *3*, 145–150.
35. Wang, X.; Qian, X.; Beitler, J. J.; Chen, Z. G.; Khuri, F. R.; Lewis, M. M.; Shin, H. J. C.; Nie, S.; Shin, D. M. Detection of Circulating Tumor Cells in Human Peripheral Blood Using Surface-Enhanced Raman Scattering Nanoparticles. *Cancer Res.* **2011**, *71*, 1526–1532.
36. Xia, X.; Yang, M.; Wang, Y.; Zheng, Y.; Li, Q.; Chen, J.; Xia, Y. Quantifying the Coverage Density of Poly(ethylene Glycol) Chains on the Surface of Gold Nanostructures. *ACS Nano* **2012**, *6*, 512–522.
37. Schlenoff, J. Zwitteration: Coating Surfaces with Zwitterionic Functionality to Reduce Nonspecific Adsorption. *Langmuir* **2014**, *30*, 9625–9636.
38. Juzenas, P.; Juzeniene, A.; Rotomskis, R.; Moan, J. Spectroscopic Evidence of Monomeric Aluminium Phthalocyanine Tetrasulphonate in Aqueous Solutions. *J. Photochem. Photobiol., B* **2004**, *75*, 107–110.
39. Lee, K.-S.; El-Sayed, M. A. Dependence of the Enhanced Optical Scattering Efficiency Relative to that of Absorption for Gold Metal Nanorods on Aspect Ratio, Size, End-Cap Shape, and Medium Refractive Index. *J. Phys. Chem. B* **2005**, *109*, 20331–20338.
40. Kim, K.-S.; Kim, J.-H.; Kim, H.; Laquai, F.; Arifin, E.; Lee, J.-K.; Yoo, S. I.; Sohn, B.-H. Switching Off FRET in the Hybrid Assemblies of Diblock Copolymer Micelles, Quantum Dots, and Dyes by Plasmonic Nanoparticles. *ACS Nano* **2012**, *6*, 5051–5059.
41. Lovell, J. F.; Chen, J.; Jarvi, M. T.; Cao, W.-G.; Allen, A. D.; Liu, Y.; Tidwell, T. T.; Wilson, B. C.; Zheng, G. FRET Quenching of Photosensitizer Singlet Oxygen Generation. *J. Phys. Chem. B* **2009**, *113*, 3203–3211.
42. Wu, C.; Peng, H.; Jiang, Y.; McNeill, J. Energy Transfer Mediated Fluorescence from Blended Conjugated Polymer Nanoparticles. *J. Phys. Chem. B* **2006**, *110*, 14148–14154.
43. Crow, J. P. Dichlorodihydrofluorescein and Dihydrorhodamine 123 Are Sensitive Indicators of Peroxynitrite *In Vitro*: Implications for Intracellular Measurement of Reactive Nitrogen and Oxygen Species. *Nitric Oxide* **1997**, *1*, 145–157.
44. Chithrani, B. D.; Chan, W. C. W. Elucidating the Mechanism of Cellular Uptake and Removal of Protein-Coated Gold Nanoparticles of Different Sizes and Shapes. *Nano Lett.* **2007**, *7*, 1542–1550.
45. Huang, P.; Lin, J.; Wang, S.; Zhou, Z.; Li, Z.; Wang, Z.; Zhang, C.; Yue, X.; Niu, G.; Yang, M.; et al. Photosensitizer-Conjugated Silica-Coated Gold Nanoclusters for Fluorescence Imaging-Guided Photodynamic Therapy. *Biomaterials* **2013**, *34*, 4643–4654.
46. Zhang, C.; Gao, S.; Jiang, W.; Lin, S.; Du, F.; Li, Z.; Huang, W. Targeted Minicircle DNA Delivery Using Folate-Poly(ethylene Glycol)-Polyethylenimine as Non-Viral Carrier. *Biomaterials* **2010**, *31*, 6075–6086.
47. Friberg, E. G.; ČunderlíKová, B.; Pettersen, E. O.; Moan, J. pH Effects on the Cellular Uptake of Four Photosensitizing Drugs Evaluated for Use in Photodynamic Therapy of Cancer. *Cancer Lett.* **2003**, *195*, 73–80.
48. Antipov, A. A.; Sukhorukov, G. B.; Donath, E.; Mohwald, H. Sustained Release Properties of Polyelectrolyte Multilayer Capsules. *J. Phys. Chem. B* **2001**, *105*, 2281–2284.
49. Kim, B.-S.; Smith, R. C.; Poon, Z.; Hammond, P. T. MAD (multiagent Delivery) Nanolayer: Delivering Multiple

Therapeutics from Hierarchically Assembled Surface Coatings. *Langmuir* **2009**, *25*, 14086–14092.
50. Hong, J.; Shah, N. J.; Drake, A. C.; DeMuth, P. C.; Lee, J. B.; Chen, J.; Hammond, P. T. Graphene Multilayers as Gates for Multi-Week Sequential Release of Proteins from Surfaces. *ACS Nano* **2012**, *6*, 81–88.
51. Oo, M. K. K.; Yang, X.; Du, H.; Wang, H. 5-Aminolevulinic Acid-Conjugated Gold Nanoparticles for Photodynamic Therapy of Cancer. *Nanomedicine (London, U. K.)* **2008**, *3*, 777–786.
52. Yang, Y.; Gao, N.; Hu, Y.; Jia, C.; Chou, T.; Du, H.; Wang, H. Gold Nanoparticle-Enhanced Photodynamic Therapy: Effects of Surface Charge and Mitochondrial Targeting. *Ther. Delivery* **2015**, *6*, 307–321.
53. Yang, Y.; Hu, Y.; Du, H.; Wang, H. Intracellular Gold Nanoparticle Aggregation and Their Potential Applications in Photodynamic Therapy. *Chem. Commun. (Cambridge, U. K.)* **2014**, *50*, 7287–7290.
54. Khaing Oo, M. K.; Yang, Y.; Hu, Y.; Gomez, M.; Du, H.; Wang, H. Gold Nanoparticle-Enhanced and Size-Dependent Generation of Reactive Oxygen Species from Protoporphyrin IX. *ACS Nano* **2012**, *6*, 1939–1947.